ACS Catalysis

Research Article

pubs.acs.org/acscatalysis

Electrodeposited Ultrafine NbO_x, ZrO_x, and TaO_x Nanoparticles on Carbon Black Supports for Oxygen Reduction Electrocatalysts in Acidic Media

Jeongsuk Seo,[†] Dongkyu Cha,[‡] Kazuhiro Takanabe,[§] Jun Kubota,[†,⊥] and Kazunari Domen*[,†]

[†]Department of Chemical System Engineering, The University of Tokyo, 7-3-1 Hongo, Bunkyo-ku, Tokyo 113-8656, Japan

[‡]Advanced Nanofabrication, Imaging and Characterization Laboratory, King Abdullah University of Science and Technology (KAUST), Thuwal 23955-6900, Saudi Arabia

[§]Division of Physical Sciences and Engineering, KAUST Catalysis Center (KCC), King Abdullah University of Science and Technology (KAUST), 4700 KAUST, Thuwal, 23955-6900 Saudi Arabia

[⊥]Elements Strategy Initiative for Catalysts and Batteries (ESICB), Kyoto University, Katsura, Kyoto 615-8520, Japan

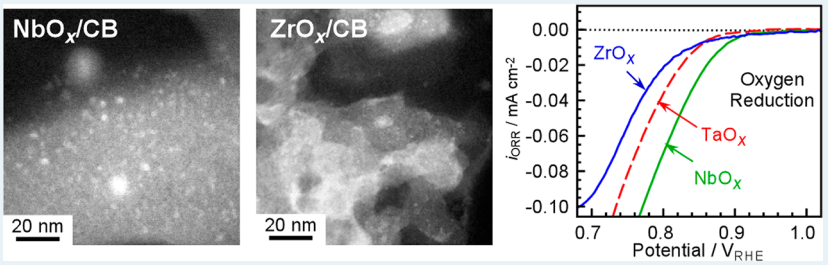

ABSTRACT: A remarkable electrocatalytic activity was obtained for the oxygen reduction reaction (ORR) in acidic solutions on ultrafine nano-oxide catalysts based on group IV or V elements. By potentiostatic electrodepostion in nonaqueous solutions at 298 K followed by heat treatment in H_2 gas, highly dispersed fine nanoparticles of NbO_x, ZrO_x, and TaO_x with sizes of less than 5 nm were prepared and deposited on carbon black (CB) loaded electrodes. These oxide nanoparticles showed high catalytic activities with high onset potentials of 0.96 V_{RHE} (NbO_x), 1.02 V_{RHE} (ZrO_x), and 0.93 V_{RHE} (TaO_x) for the ORR. Owing to the high chemical stability of group IV and V oxides, the catalysts were very stable during the ORR in acidic solutions. Surface characterization and chemical identification were performed using scanning transmission electron microscopy (STEM), energy dispersive X-ray spectroscopy (EDS), and X-ray photoelectron spectroscopy (XPS). All results clearly indicate the formation of nano-oxide electrocatalysts that show an outstanding ORR performance, whereas the bulk oxides are not active because of the absence of electronic conductivity. The present work demonstrates potential candidates for highly stable, non-noble-metal cathode catalysts for polymer electrolyte fuel cells (PEFCs), where the catalysts are exposed to highly acidic and oxidizing conditions.

KEYWORDS: *PEFCs, nonplatinum catalysts, electrodeposition, Nb_2O_5, ZrO_2, Ta_2O_5, oxygen reduction reaction*

1. INTRODUCTION

Owing to the low abundance and high cost of the Pt and Pt-based materials currently used as electrocatalysts in polymer electrolyte fuel cells (PEFCs), many promising alternative cathode materials with a reasonable activity for the oxygen reduction reaction (ORR) have been explored.[1−5] Group IV and V transition metals are known to be chemically stable under the acidic conditions of a typical PEFC cathode atmosphere. Thus, several Ti-, Zr-, Ta-, and Nb-based compounds have been reported as ORR electrocatalysts.[5−13] These were mostly nitrides, carbides, oxides, and mixed compounds, that were doped with additional elements or subjected to various heat treatments to improve their electrocatalytic properties for the ORR. However, the catalysts studied to date have shown limited catalytic activity and/or poor long-term stability for PEFC applications. Although nitrides, and N-doped compounds in particular, have exhibited high conductivity and excellent ORR activity, they have a strong tendency to be transformed into oxides under acidic PEFC conditions.[5,9] In fact, oxides have been reported to be the most stable materials in an acidic atmosphere.[14−16] The Pourbaix electrochemical equilibrium diagrams for group IV or V elements explain that the oxides are chemically stable under pH and applied potentials corresponding to the typical PEFC operation conditions.[15] Sasaki et al. has also suggested that, according to their thermochemical calculation, the oxides are determined as the most stable substances at pH = 0 and 353 K.[16] Nevertheless, the most stable oxides with a maximum

Received: July 8, 2013
Revised: August 15, 2013
Published: August 16, 2013

valence are an insulator in bulk, which indicates that they might have low ORR activity.

With this background, we studied metal oxide catalysts with no nitrogen or carbon doping based on group IV or V elements as nonplatinum PEFC cathode electrocatalysts. To improve their poor electrical conductivity, our approach has been to use ultrafine oxide nanoparticles, which have yet to be fully researched. Hence, it is very hard to control the particle size of oxides with conventional methods.[7,11,17,18] This is because catalyst particles easily aggregate and grow to sizes of more than 100 nm during high temperature calcination. Thus, the fabrication of metal oxide nanoparticles has been attempted by electrodeposition at room temperature. Electrodeposition is a very useful method for controlling the particle size and shape of catalysts and distributing them uniformly on conductive materials such as carbon black.[19−21] With the exception of certain specific complexes, group IV or V metal compounds are difficult to dissolve in aqueous solutions because they precipitate into oxides or hydroxides by reacting with H_2O. Metal cations cannot be reduced on well-grown metal oxide particles because of the lower conductivity of these oxides, with the result that small particles become widely dispersed on the substrate surface. Thus, our group has recently reported that highly dispersed TaO_x nanoparticles, 2−3 nm in size, could be prepared by electrodeposition in an ethanol-based Ta plating bath at room temperature, and these fine oxide nanoparticles showed excellent catalytic activity for the ORR.[22,23]

In the present work, we have extended the study of nanoparticle oxides for high ORR catalytic performance to the group IV and V elements Ta, Nb, and Zr. Highly dispersed NbO_x, ZrO_x, and TaO_x nanoparticles were successfully deposited on carbon black (CB) supports by potentiostatic electrodeposition in nonaqueous metal ethoxide-based solutions. These oxide nanoparticles were characterized in terms of their physical properties and electrocatalytic performance for the ORR. To improve the physical properties and electrocatalytic performance, the deposition conditions were optimized and surface modification was performed by H_2 treatment. Tafel slopes for the ORR were measured for the electrodeposited NbO_x, ZrO_x, and TaO_x electrodes.

2. EXPERIMENTAL SECTION

2.1. Preparation of Metal Oxide Catalysts by Electrodeposition. First, bare CB electrodes were prepared as substrates for electrodeposition, using a CB powder. The CB powder (Vulcan-XC72) was mixed with a Nafion ionomer solution (Aldrich 1100EW, 5 wt % in water/aliphatic alcohols) and isopropyl alcohol (IPA, 99.9%, Kanto Chemical). The proportion of CB to ionomer solution was adjusted to 2:3 by weight. The mixture was repeatedly ultrasonicated and magnetically stirred to ensure a good dispersion. The resultant well-dispersed CB slurry was sprayed onto carbon paper (EC-TP1-060T, Toyo Corporation, treated by polytetrafluoroethylene (PFEC)) at 343 K. The loading amounts of the CB layers were fixed at 0.5 mg cm^{-2}. After spraying, the bare CB electrodes were completely dried to evaporate the residual solvent. Second, the electrodeposition of Nb, Zr, and Ta species was performed in a three-electrode system with a potentiostat (HZ5000, Hokuto Denko). A bare CB electrode with an area of 1 cm^2 served as the working electrode. A carbon rod was used as a counter electrode to prevent Pt contamination. An Ag/AgCl electrode (HX-R4, Hokuto Denko) was mounted as a reference electrode. The three electrodes were immersed in nonaqueous metal ethoxide-based solutions at 298 K. The nonaqueous plating bath for electrodeposition consisted of metal precursors, 20 or 100 mM $NbCl_5$, $ZrCl_4$, and $TaCl_5$, (Kanto Chemical), a supporting electrolyte of 20 mM $NaClO_4$ (99%, Sigma-Aldrich), and an anhydrous ethanol solvent. A constant potential was applied to the bare CB electrode for 10 s at 298 K during each electrodeposition process. After electrodeposition, the electrodes were washed with ethanol to remove the residues of the metal precursors and were thoroughly dried. Finally, the as-electrodeposited electrodes were heated at a rate of 5 K min^{-1} to 473, 523, 553, or 573 K under a pure H_2 flow and kept at that temperature for 30 min.

2.2. Electrochemical Measurements. The deposition behavior of metal ethoxides was studied on a glassy carbon (GC) electrode under the same environment with a nonaqueous plating solution and a standard three-electrode system for electrodeposition. A carbon rod was used as a counter electrode to avoid Pt contamination, and an aqueous Ag/AgCl electrode was used as a reference electrode. At the beginning of the cathodic sweep, cyclic voltammetry for the reduction reaction of metal complexes was performed over the potential range from 1.0 to −1.0 $V_{Ag/AgCl}$ under an Ar-purged atmosphere at 298 K. Cyclic voltammograms (CVs) were recorded at a scan rate of 5 mV s^{-1}.

To measure the ORR activity of the electrodeposited oxide nanoparticles, electrochemical measurements were carried out in a conventional single-vessel electrochemical cell with an Ag/AgCl reference electrode and carbon counter electrodes. Linear sweep voltammograms (LSVs) for the ORR were obtained from 1.23 to 0.20 V_{RHE} with a scan rate of 5 mV s^{-1} in a 0.1 M aqueous H_2SO_4 solution at 298 K while purging with Ar and O_2 at 1 atm. The difference in current density between the O_2-saturated and Ar-saturated atmospheres was considered to correspond exactly to the real catalytic activity for ORR, i_{ORR}. The area for density estimation is the geometric area of carbon sheets loaded with the catalysts. The Ag/AgCl reference electrode was calibrated in a 0.1 M aqueous H_2SO_4 solution at 298 K to a reversible hydrogen electrode (RHE) consisting of a Pt electrode and H_2 at 1 atm; the potential in the 0.1 M H_2SO_4 solution in this paper is expressed in RHE as V_{RHE}.

2.3. Catalyst Characterization. The surface morphology and elemental composition of the electrodeposited oxide electrodes were characterized by scanning transmission electron microscopy (STEM; Titan ST, FEI), scanning electron microscopy (SEM; S-4700, HITACHI), and energy dispersive X-ray spectroscopy (EDS; EMAX-7000, Horiba). The loading amounts of the Nb, Zr, and Ta on the CB electrode were determined by inductively coupled plasma atomic emission spectroscopy (ICP-AES). The chemical identity and modified surface structure of the oxide electrodes were analyzed by X-ray photoelectron spectroscopy (XPS; JPS-90SX, JEOL) using a nonmonochromatized X-ray source with a Mg Kα anode, at an emission current of 10 mA and an acceleration voltage of 8 kV. The binding energies were calibrated using Au4$f_{7/2}$ at 83.8 eV to compensate for electrostatic charging.

3. RESULTS AND DISCUSSION

3.1. Electrodeposition Behavior of Metal Precursors on Glassy Carbon. The electrochemical behavior of Nb and Zr species on glassy carbon (GC) was examined for metal ethoxide-based nonaqueous solutions under an Ar-saturated atmosphere. In our previous studies, Ta was investigated in detail using a $TaCl_5$ ethanol solution purged under Ar gas.[22,23]

Here, nonaqueous metal ethoxide solutions were selected to avoid the production of metal oxides as a result of the direct reaction between the precursor and H_2O. The electrodeposition plating bath was prepared by dissolving $NbCl_5$, $ZrCl_4$, or $TaCl_5$ powder in ethanol (20 mM). $NaClO_4$ (20 mM) was also added to each solution as a supporting electrolyte. GC electrodes with an area of 1 cm^2 were used as the substrate for electrodeposition.

Figure 1 shows the CVs of GC electrodes in $NbCl_5$, $ZrCl_4$, and $TaCl_5$ ethanol solutions and a blank solution without any

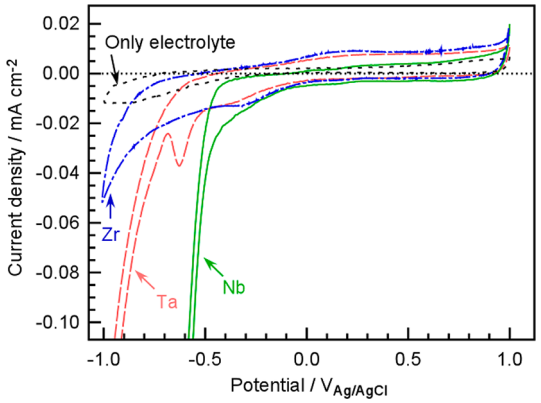

Figure 1. Cyclic voltammograms of GC electrodes in nonaqueous metal ethoxide plating baths between 1.0 and −1.0 $V_{Ag/AgCl}$ measured at a sweep rate of 5 mV s^{-1} in an Ar-saturated atmosphere at 298 K. The dotted black line was measured as a blank under the supporting electrolyte solution without the metal precursors, 20 mM $NaClO_4$ in ethanol. The three electrodeposition plating baths contained 20 mM $NbCl_5$ (solid green), $ZrCl_4$ (dashed-dotted blue), and $TaCl_5$ (dashed red) as metal precursors and the electrolyte solution.

metal precursors under an Ar-saturated environment at 298 K. The $NbCl_5$, $ZrCl_4$, and $TaCl_5$ species dissolved to form ethoxides or chlorides partly substituted by ethoxides. The CVs were measured starting with a cathodic sweep, over the potential range from −1.0 to 1.0 $V_{Ag/AgCl}$ at a scan rate of 5 mV s^{-1}. For an ethanol solution without metal precursors (black dotted line in Figure 1), most of the current can be assigned to the non-Faradaic current, owing to the electric double layer. The small cathodic current below −0.25 $V_{Ag/AgCl}$ is presumably attributable to the formation of H_2 from the H_2O impurity in $NaClO_4$ or ethanol or the reduction of surface functional groups on the carbon substrate. The solutions containing metal species gave clearly distinguishable reduction peaks. The cathodic current was measured gradually from around 0 $V_{Ag/AgCl}$ in all cases, but different potentials were required to obtain prominent cathodic peaks for each metal species. In the case of the Ta precursor, our previous report identified two reduction peaks, positioned at −0.35 and −0.63 $V_{Ag/AgCl}$, corresponding to the reduction of Ta(V) to Ta metal via Ta(IV) and Ta(III), respectively.[22,23] The curve for the Nb precursor showed a sharp current increase below −0.4 $V_{Ag/AgCl}$ in the cathodic sweep. In addition, a broad shoulder was observed in the cathodic current for the Nb precursor roughly between −0.2 and −0.3 $V_{Ag/AgCl}$. In the reverse sweep, a small oxidation current appeared from 0.1 $V_{Ag/AgCl}$, as a result of incomplete stripping of Nb species deposited on the GC during the cathodic scan. For the Zr plating solution, a broad reduction peak was observed at −0.3 $V_{Ag/AgCl}$ and the cathodic current gradually increased. The subsequent anodic sweep also caused the electrodeposited GC to show an oxidation current above −0.25 $V_{Ag/AgCl}$ due to incomplete stripping of Zr species alike on the Ta-electrodeposited GC. The increase in the cathodic current around −0.5 $V_{Ag/AgCl}$ (Nb), −0.8 $V_{Ag/AgCl}$ (Ta), and −1.0 $V_{Ag/AgCl}$ (Zr) is thought to be mainly due to H_2 evolution from the protons of HCl, generated by the substitution of the chloride in the metal precursor by ethoxide. Practically, the gas bubbles were observed on the electrodes by the eyes at such potentials. The currents and potentials for H_2 evolution were different for each metal complex, clearly indicating that the HCl concentrations differed because of the difference in the stability of the metal complexes.

The standard reduction potentials for Nb^{5+}, Ta^{5+}, and Zr^{4+} to their metallic states are −0.65, −0.81, and −1.55 V_{SHE}, respectively, in which SHE stands for a standard hydrogen electrode.[24] Thus, the applied potentials of −0.4 to −0.5 $V_{Ag/AgCl}$ for our deposition conditions at 298 K cannot reduce these metal cations to the neutral metallic state. In the case of Ta, we have concluded that the cathodic current at −0.35 and −0.63 $V_{Ag/AgCl}$ reduces Ta(V) to Ta(IV) and Ta(III), leading to the attachment of the Ta precursor to the carbon substrate. In the case of Nb and Zr, the broad peak or shoulder above −0.5 $V_{Ag/AgCl}$ (Nb) and −1.0 $V_{Ag/AgCl}$ (Zr) should be attributed to the cathodic current for the partial reduction of Nb(V) and Zr(IV) to lower valence states. The coexistence of the byproduct HCl in the deposition bath would give certain influences on the electrodeposition of the metal cation species.[23] Therefore, separate experiments directly using pure metal ethoxide precursors resulted in too large particles of metal oxide, leading to a poor ORR activity, as is the case for bulk oxides. The formation of highly dispersed oxide particles might be due to the presence of protons and chloride ions in the ethanol solution. The effect of coexisting ions in the solution during electrodeposition remains unclear.

As will be discussed in Section 3.4, the cathodically electrodeposited species on CB surfaces from $NbCl_5$, $ZrCl_4$, and $TaCl_5$ ethanol solutions were mostly oxidized to their highest valence in air after electrodeposition. The formation of nitrides or carbides is unlikely, so that the Nb, Zr, and Ta species were presumably oxides or hydroxides. These electrodes did not show any X-ray diffraction peaks, and the chemical environment of the Nb, Zr, and Ta species could not be identified. Thus, we express these species as NbO_x, ZrO_x, and TaO_x in this Article.

3.2. ORR Activities of NbO_x Nanoparticles Electrodeposited on Carbon Black. First, electrodeposition of Nb species was attempted by varying the potential from −0.2 to −1.0 $V_{Ag/AgCl}$ at increments of 0.1 $V_{Ag/AgCl}$, in a 20 mM $NbCl_5$ ethanol solution at 298 K, based on the deposition behavior of Nb in Figure 1. The potentials were applied for 5, 10, or 20 min. The deposition potential and time for NbO_x were optimized to obtain the highest onset potential for the ORR. The optimal conditions were found at −0.4 $V_{Ag/AgCl}$ for 10 s. The amount of Nb electrodeposited at −0.4 $V_{Ag/AgCl}$ in 10 s was estimated to be ca. 0.018 mg cm^{-2} by ICP-AES. The variation in the deposited amount of TaO_x nanoparticles has been reported in our previous paper,[23] and the optimal conditions of NbO_x and ZrO_x are determined by the similar phenomena to that of TaO_x.

For the electrodeposited TaO_x nanoparticles, the heat treatment in H_2 gas after electrodeposition was the most critical factor in improving the ORR performance.[22,23] Given the effect of H_2 treatment in modifying the electrode surface,

dx.doi.org/10.1021/cs400525u | ACS Catal. 2013, 3, 2181−2189

the Nb-electrodeposited electrodes treated under various heating temperatures were assessed with regard to catalytic activity for the ORR. The Nafion ionomer is effective as a binder for the CB electrode, but it limits the heating temperature to less than 600 K, roughly the melting point of Nafion. Figure 2A shows CVs for NbO_x electrodes electro-

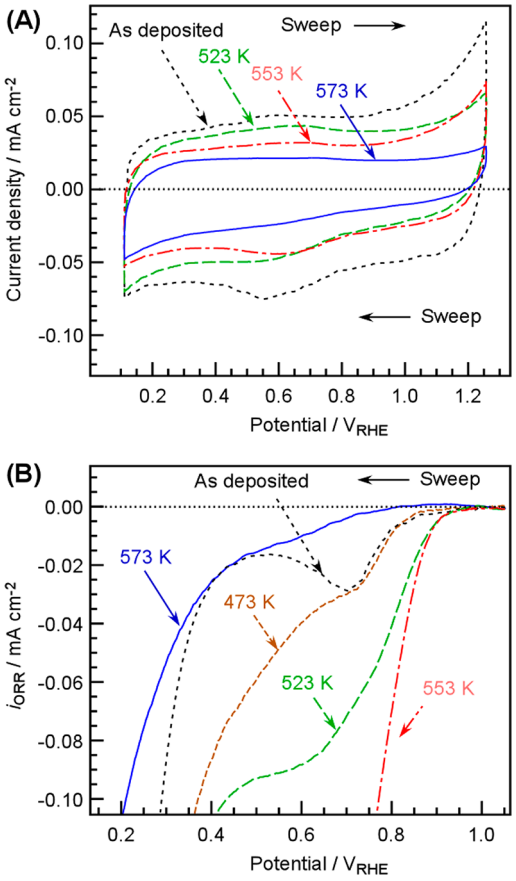

Figure 2. (A) Cyclic voltammograms of NbO_x/CB electrocatalysts in 0.1 M H_2SO_4 saturated with Ar. The catalyst was prepared by electrodeposition at −0.4 $V_{Ag/AgCl}$ for 10 s followed by H_2 treatment at 523, 553, and 573 K for 30 min. The CVs were recorded over the potential range of 1.23−0.1 V_{RHE} at a scan rate of 5 mV s^{-1} in Ar-saturated atmosphere. (B) Linear sweep voltammograms of NbO_x/CB electrocatalysts in 0.1 M H_2SO_4 at 298 K, as-deposited and treated under H_2 at 473, 523, 553, and 573 K for 30 min. The vertical axis reflects the difference in current density between the Ar and O_2 atmospheres. The potential was swept cathodically at a scan rate of 5 mV s^{-1}.

deposited on CB at −0.4 $V_{Ag/AgCl}$ in 10 s, untreated and H_2-treated at 523, 553, or 573 K for 30 min in a 0.1 M H_2SO_4 solution purged by Ar gas at 298 K. None of the polarization curves for Nb-based catalysts show any specific redox peaks in an Ar-saturated H_2SO_4 solution, unlike other group IV−V transition metal-based catalysts.[25−27] The charging current in the capacitance of the electrical double layer decreased after the H_2 treatment, probably due to the decrease in the interfacial area between the electrode and solution.[23] However, the electrodeposited NbO_x electrode decreased significantly in capacitance after treatment at 573 K, which is ascribable to undesirable disorder in the CB structure induced by heating, which decreases its surface area.[23]

Figure 2B shows LSVs for the NbO_x electrodes electrodeposited on CB at −0.4 $V_{Ag/AgCl}$ for 10 s, untreated and H_2-treated at 473, 523, 553, or 573 K for 30 min in a 0.1 M H_2SO_4 solution purged by Ar gas at 298 K. The current density, i_{ORR}, on the vertical axis indicates the difference in current density, which based on the geometric substrate area, measured between O_2-saturated and Ar-saturated atmospheres. The as-electrodeposited NbO_x electrodes showed a cathodic current for the ORR at a more negative value than 0.94 V_{RHE} (−2 μA cm^{-2}). However, the current was very small in the typical operation potential range of 0.6−0.7 V_{RHE} for PEFCs,[28] where only a single peak was measured at 0.7 V_{RHE}. With increasing heat-treatment temperature, the ORR current for NbO_x electrodes increased significantly, but it decreased above 553 K. Among the samples studied, the sample treated at 553 K showed the highest ORR current with the highest onset potential of 0.96 V_{RHE} (for −2 μA cm^{-2}). In contrast, the treatment at 573 K led to a decrease in the ORR current, and even the current at 0.2 V_{RHE} was only −0.1 mA cm^{-2}. The dramatically decreased current in the case of the treatment at 573 K presumably resulted from excessive thermally induced changes in the catalyst layers. These temperatures are close to the glass-transition temperature for Nafion, and the treatment can affect the morphological structure of CB aggregates.[23]

Figure 3A shows SEM images of NbO_x electrodes, as-electrodeposited and H_2-treated at 523, 553, and 573 K. At this scale, no noticeable difference in the shape and morphology of the CB electrodes was observed. Although no Nb species can be observed in these images, the EDS spectrum shown in

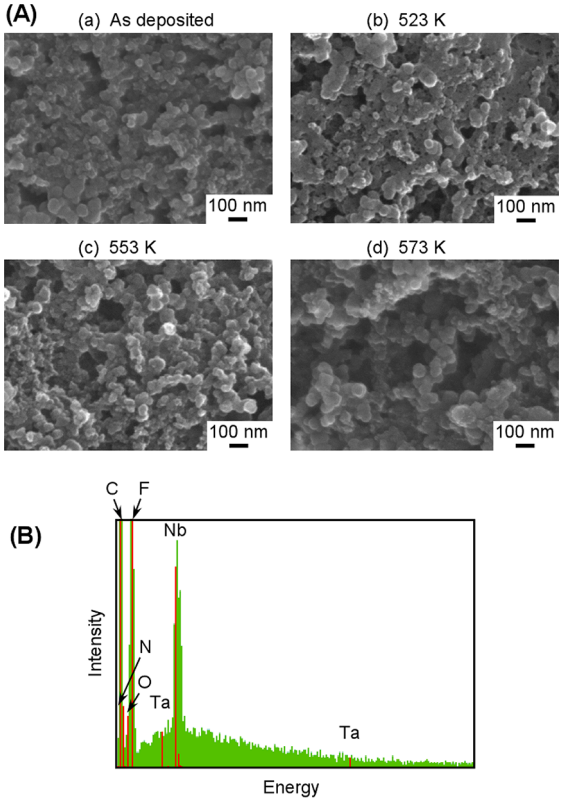

Figure 3. (A) SEM images of NbO_x catalysts deposited on CB particles before (a) and after H_2 treatment at 523 (b), 553 (c), and 573 K (d) for 30 min. (B) EDS spectrum of as-deposited NbO_x catalyst. Red lines indicate the reference position of each element.

dx.doi.org/10.1021/cs400525u | ACS Catal. 2013, 3, 2181−2189

Figure 3B confirmed its existence. This suggests that the NbO_x particles were dispersed on the CB surface in a much smaller size level (as will be discussed in Section 3.5), and the difference in catalytic performance induced by the heat treatment did not stem from an obvious structural change at a macroscopic level. A postelectrodeposition H_2 treatment has been found to clean the catalyst surface, removing organic species from the surface, as determined in a previous study using XPS.[23] Treatment at the appropriate temperature is key to obtaining the best performance.

3.3. ORR Activities of ZrO_x Nanoparticles Electrodeposited on Carbon Black. Of the group IV metals, we attempted to fabricate ZrO_x nanoparticles using electrodeposition. The ZrO_x catalysts were prepared by electrodeposition of Zr species on bare CB electrodes at −0.5 $V_{Ag/AgCl}$ for 10 s in a $ZrCl_4$ ethanol solution at 298 K. Subsequently, the as-electrodeposited electrodes were treated by heating in H_2 gas. In the same manner as the NbO_x catalysts, the H_2 treatment conditions were optimized and set at 473 K for 30 min. Figure 4A shows the CVs for the electrodeposited ZrO_x electrodes in Ar before and after the H_2 treatment. No specific redox peak is observed, as in the CVs of typical zirconium oxide electrodes.[27,29] After the H_2 treatment, the ZrO_x electrode showed a decrease in the double-layer capacitance, as in the case of the NbO_x electrode (Figure 2A).

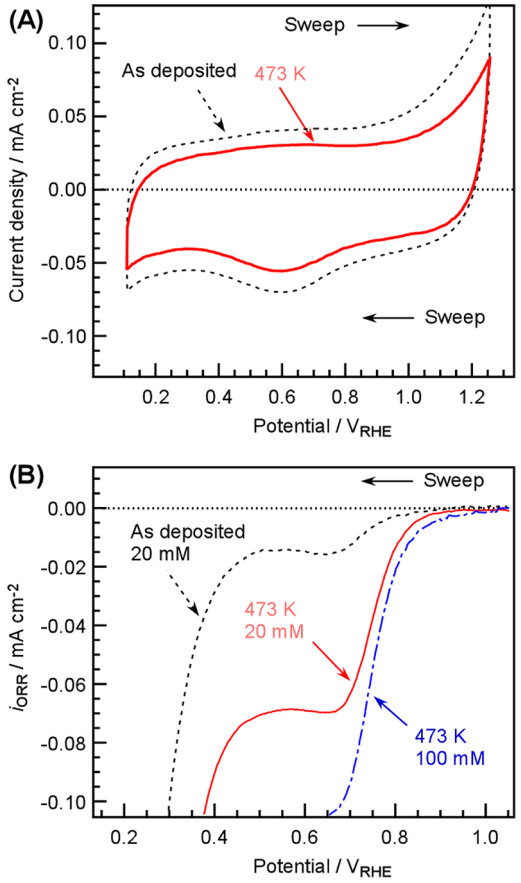

Figure 4. (A) Cyclic voltammograms of ZrO_x catalysts in 0.1 M H_2SO_4 saturated with Ar. The catalyst was prepared by electrodeposition at −0.5 $V_{Ag/AgCl}$ for 10 s in 20 mM $Zr(OC_2H_5)_4$ solution before and after H_2 treatment at 473 K for 30 min. The CVs were recorded from 1.23 to 0.1 V_{RHE} at a scan rate of 5 mV s^{-1} in Ar-saturated atmosphere. (B) Linear sweep voltammograms of ZrO_x/CB electrocatalysts in 0.1 M H_2SO_4 at 298 K, electrodeposited in 20 and 100 mM $Zr(OC_2H_5)_4$ solutions, as-deposited and H_2-treated at 473 K for 30 min. The vertical axis reflects the difference in current density between the Ar and O_2 atmospheres. The potential was cathodically swept at a scan rate of 5 mV s^{-1}.

LSVs were examined to assess ORR activities on ZrO_x electrodes electrodeposited in 20 and 100 mM $ZrCl_4$ ethanol solutions before and after H_2 treatment (see Figure 4B). Catalysts electrodeposited in the 20 mM $ZrCl_4$ ethanol solution clearly showed catalytic activity for the ORR. After H_2 treatment at 473 K, the current increased and the onset potential was 0.96 V_{RHE}. The ORR polarization curves for untreated and H_2-treated ZrO_x electrodes prepared from 20 mM $ZrCl_4$ exhibited a mass-transfer limiting current of ∼15 and ∼70 $\mu A\ cm^{-2}$, respectively, around a potential of 0.5−0.6 V_{RHE}. Subsequently, the current increased sharply again in the lower potential region. We determined the loading amounts of Zr on the CB electrode by ICP-AES analysis. Zr was detected at an amount of ca. 0.003 mg cm^{-2}, which is six times lower than that for the Nb electrodeposits, even under an optimal deposition condition. The appearance of the limiting current over 0.5−0.6 V_{RHE} can presumably be linked to the small loading amount of ZrO_x. The subsequent current increase below the limiting current might be due to reactions on the CB surfaces because CB showed an onset potential of 0.45 V_{RHE} for ORR.[23] Thus, electrodeposition was performed with a higher loading of Zr, using a more concentrated 100 mM $ZrCl_4$ solution. The amount deposited increased by a factor of around 2.3 to 0.007 mg cm^{-2}, even though the Zr precursor concentration was 5 times higher. Figure 4B also shows the ORR polarization curves for the H_2-treated ZrO_x electrode that was electrodeposited in a 100 mM $ZrCl_4$ ethanol solution. The ORR current for the ZrO_x electrode electrodeposited in 100 mM $ZrCl_4$ was found to be significantly higher than that for the electrode electrodeposited in the more dilute solution, and the onset potential of the former was 1.02 V_{RHE}. These results suggest that the ZrO_x electrodes have the highest onset potential for the ORR in the present study, comparable to that of a commercial Pt/CB catalyst.

3.4. Surface Chemical States of the Electrodeposited Metal Oxides. For the NbO_x and ZrO_x catalysts, the chemical states of the surface of electrodeposited NbO_x and ZrO_x were investigated by XPS. Figure 5 displays narrow-scan Nb 3d (A) and Zr 3d (B) XPS spectra for the NbO_x and ZrO_x electrodes, which were electrodeposited at −0.4 and −0.5 $V_{Ag/AgCl}$ for 10 s in 20 mM $NbCl_5$ and 100 mM $ZrCl_4$ solutions, followed by a H_2 treatment at 553 and 473 K for 30 min, respectively. The XPS spectra did not change before and after the ORR measurements. These conditions were selected to obtain the highest ORR activity, as discussed in Sections 3.2 and 3.3. The chemical shifts corresponding to the binding energies of metallic Nb and Zr and fully oxidized Nb_2O_5 and ZrO_2 are also shown in Figure 5. The XPS spectra deviated from the typical double split peaks corresponding to Nb_2O_5 and ZrO_2. Accordingly, the broad Nb 3d spectrum was deconvoluted into oxidation states labeled Nb_2O_5 (Nb^{5+}), NbO_2 (Nb^{4+}), and NbO (Nb^{2+}) on the basis of previous reference data.[30−32] It was assigned to the peak positions of Nb $3d_{5/2}$ for the three different oxidation components to 209.7, 208.3, and 204.0 eV. The spin−orbit doublet separation at 2.8 eV and the fwhm of 2.0 ± 0.1 eV for all Nb 3d states were used to obtain the best fit. Next, we also attempted to deconvolute the atypical Zr 3d spectrum using two oxidation states, ZrO_2 (Zr^{4+}) and ZrO_x

dx.doi.org/10.1021/cs400525u | ACS Catal. 2013, 3, 2181−2189

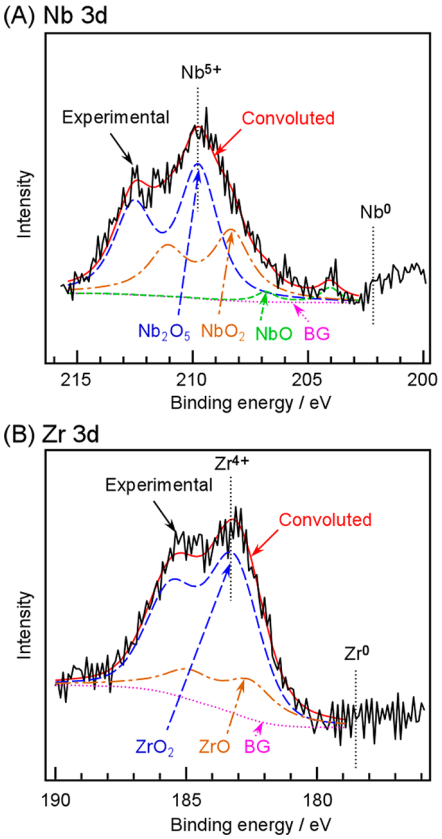

Figure 5. Narrow scanned XPS spectra for (A) Nb 3d and (B) Zr 3d of electrodeposited NbO_x/CB and ZrO_x/CB electrocatalysts after H_2 treatment at 553 and 473 K for 30 min, respectively. The deconvoluted peaks corresponding to each valence cation are shown.

$(Zr^{3+,\,2+})$.[33−35] The intense doublet at 184.2 eV and the relatively small doublet at 182.5 eV were ascribed, respectively, to Zr $3d_{5/2}$ for pure ZrO_2 and a suboxide ZrO_x. The spin−orbit doublet separation at 2.39 eV and the fwhm of 2.2 ± 0.1 eV for all Zr 3d species made the Zr 3d spectrum a highly suitable fit. Both convolutions clearly indicate that the electrodeposited Nb and Zr species consisted of several oxidation states. Moreover, the most abundant states were Nb_2O_5 (60%) and ZrO_2 (77%). The metal species were cathodically electrodeposited on CB electrodes and heat-treated in reducing H_2 gas. The preparation procedure ensured that the electrodeposited oxides had lower oxidation states than Nb^{5+} or Zr^{4+}. These XPS results resemble those for TaO_x electrodes in our previous work.[23] The electrodeposited TaO_x nanoparticles mainly consisted of the highest oxidized species with some reduced species remaining. These electrodeposited electrodes did not show X-ray diffraction patterns, indicating that the oxide species were amorphous or highly dispersed. Thus, the oxide catalysts prepared by electrodeposition are noted in this paper as NbO_x, ZrO_x, and TaO_x.

3.5. STEM Images of NbO_x and ZrO_x Nanoparticles on CB. The surface morphology of the electrodeposited NbO_x and ZrO_x catalysts was investigated using STEM. Figure 6 shows STEM images of NbO_x (A) and ZrO_x (B) nanoparticles electrodeposited on CB particles under deposition conditions corresponding to those for Figure 5. Figure 6A confirms that the bright particles, the electrodeposited NbO_x, were very uniformly distributed on the CB surface and had a size of about 2−3 nm. In contrast, there are very few ZrO_x particles

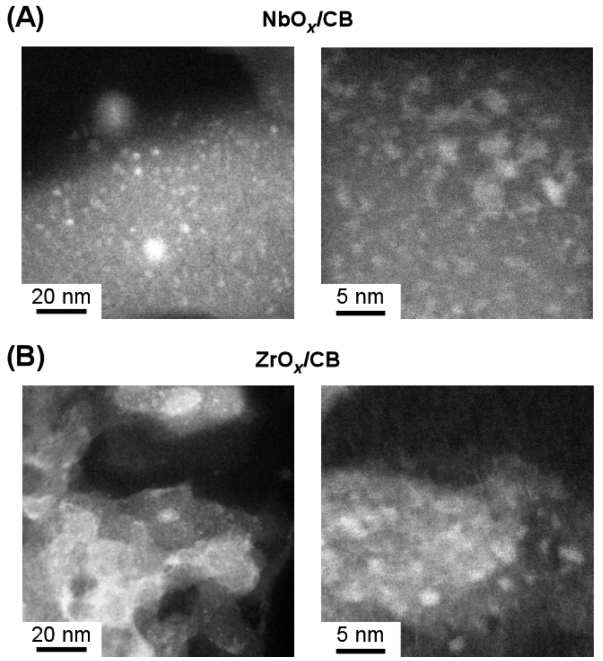

Figure 6. STEM images of (A) NbO_x and (B) ZrO_x nanoparticles electrodeposited on CB, taken at two different magnifications.

(brightest spots) in Figure 6B because there was less deposition than in the case of NbO_x. However, the magnified image in Figure 6B reveals that the ZrO_x particles (again, the brightest spots) were well dispersed on the CB surface and had a size of 1−2 nm. Overall, the electrodeposition method could be successfully used to fabricate NbO_x and ZrO_x electrodes on CB by preparing highly dispersed particles with an average size of 2 nm. These uniform nanoparticle dispersions enabled the formation of efficient active sites with high onset potential and a significantly high current for the ORR.

We believe that the advantage of electrodeposition over other preparation methods is its capability to fabricate nanoscale oxide particles. In the case of a conventional method such as impregnation, the metal precursor molecules easily agglomerate during condensation of the solvent. In the case of electrodeposition, the metal precursor can adhere to and be reduced on small, electroconductive oxide particles or the bare CB surface. The growth of oxide particles automatically stops when their electroconductivity starts to decrease. Thus, small oxide nanoparticles having a certain electroconductivity could be deposited on the CB surface with a high degree of dispersion, and the particle layer thickness on the CB surface was no more than a few nanometers.

3.6. Comparison of the ORR Activities of NbO_x, ZrO_x, and TaO_x. Figure 7 shows the LSVs for NbO_x, ZrO_x, and TaO_x electrodes electrodeposited under optimal conditions. Table 1 tabulates their onset potentials, cathodic current densities at 0.7 V_{RHE} for the ORR, and deposition amounts. The result for a commercial Pt/CB catalyst, 20 wt % Pt/CB powder sprayed onto the bare carbon electrode with loading amount of 0.025 mg cm^{-2}, is shown as a reference.[23] The NbO_x, ZrO_x, and TaO_x nanoparticles showed high onset potential for the ORR comparable to the Pt/CB catalyst although the current densities were lower. The ZrO_x catalysts showed the highest onset potentials and were followed by NbO_x and TaO_x, in that order. This trend in onset potential can be understood along with the intrinsic activity of a number of active sites for the ORR. Several

dx.doi.org/10.1021/cs400525u | ACS Catal. 2013, 3, 2181−2189

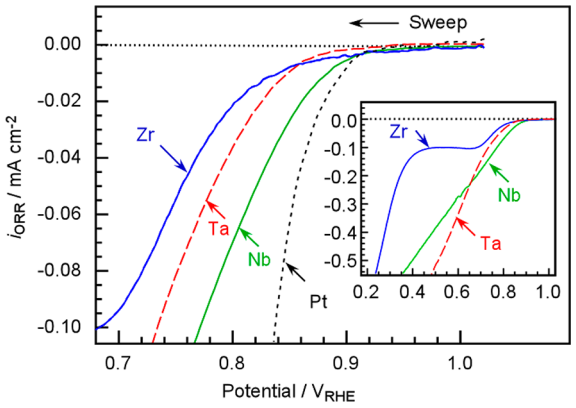

Figure 7. Linear sweep voltammograms of electrodeposited NbO_x/CB (solid green), ZrO_x/CB (solid blue), and TaO_x/CB (dashed red) catalysts in 0.1 M H_2SO_4 at 298 K. NbO_x/CB, ZrO_x/CB, and TaO_x/CB were electrodeposited at −0.4, −0.5, and −0.5 $V_{Ag/AgCl}$ for 10 s and then treated under H_2 at 553, 473, and 523 K for 30 min, respectively. The vertical axis reflects the difference in current density between the Ar and O_2 atmospheres. The inset shows the wider range of voltammograms. The potential was swept cathodically at a scan rate of 5 mV s^{-1}. A result for a commercial 20 wt % Pt/CB is shown as a reference.[21]

Table 1. Onset Potential, Current Density, and Loading Amount of Ta, Nb, and Zr Oxide Nanoparticles Prepared by Electrodeposition on CB[a]

catalyst	onset potential for −2 μA cm^{-2} (V_{RHE})	current density at 0.7 V_{RHE} (mA cm^{-2})	loading amount (metal-mg cm^{-2})
TaO_x/CB	0.93	0.15	0.016
NbO_x/CB	0.96	0.18	0.018
ZrO_x/CB	1.02	0.09	0.007

[a]The onset potential and current density were obtained for ORR in 0.1 M H_2SO_4 at 298 K. The amounts of electrodeposited Ta, Nb, and Zr were determined by ICP-AES.

researchers have reported the adsorption energy of oxygen on many transition metals.[4,36,37] Specifically, Miyazaki et al. published the heats of adsorption and bond energies for oxygen on various transition metals.[36] On the basis of these results, the oxygen adsorption enthalpies on Zr, Nb, and Ta were calculated to be 824, 832, and 937 kJ mol^{-1}, respectively.[4] The atomic oxygen adsorption properties of metal surfaces indirectly reflect the activation of oxygen in the ORR. The important role of molecularly adsorbed oxygen, which desorbed from 120 to 170 K from the catalysts, has also been proposed in the previous papers,[5,38] and the molecularly adsorbed oxygen, which is the precursor of the reaction, should directly reflect the activation of oxygen in the ORR. The adsorption enthalpies of atomic oxygen can be considered to positively relate to that for molecularly adsorbed oxygen. Thus, the onset potential for the electrodeposited oxides ZrO_x, NbO_x, and TaO_x related to their adsorption enthalpies. Clearly, the ZrO_x catalysts had the highest onset potential for the ORR because the oxygen affinity of Zr atoms was the smallest. However, the amount of Zr deposition was smaller than those for group V metals, so that the current at 0.7 V_{RHE} was also smaller. Generally, Zr ethoxide mainly agglomerates in solution as tetramers with octahedral 6-fold coordinated zirconium metal centers, while Nb and Ta ethoxides occur as dimers.[39−41] Fine tuning the preparation conditions and selecting the appropriate Zr complexes for the deposition bath might yield more highly loaded ZrO_x electrodes. Thus, for a high ORR activity, the development of ZrO_x electrodes with a high degree of loading would be more challenging to improve the performance for a PEFC application.

The long-term stability for the TaO_x nanoparticles in acidic media has been reported in our previous paper,[23] and the ORR current decreased only a few percent after the accelerated durability test for 1000 cycles. The ZrO_x and NbO_x catalysts also showed similar stability to TaO_x.

3.7. General Discussion on Tafel Slopes. The LSVs for NbO_x, ZrO_x, and TaO_x in Figure 7 are plotted as Tafel plots in Figure 8, where the current density is normalized to the mass-specific current using Table 1. In the present study, we limit the comparison of ORR kinetics on all oxide catalysts to the high-potential region because the effect of mass transfer could not otherwise be completely ignored under our measurement conditions. The Tafel slopes for NbO_x, ZrO_x, and TaO_x electrodes were estimated to be 66, 133, and 102 mV dec^{-1}.

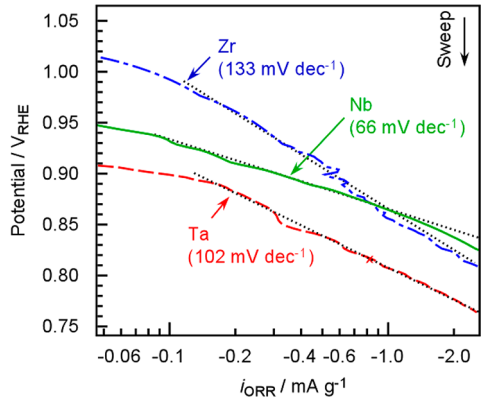

Figure 8. Tafel plots of electrodeposited NbO_x/CB (solid green), ZrO_x/CB (dashed-dotted blue), and TaO_x/CB (dashed red) catalysts in 0.1 M H_2SO_4 at 298 K. NbO_x/CB, ZrO_x/CB, and TaO_x/CB were electrodeposited at −0.4, −0.5, and −0.5 $V_{Ag/AgCl}$ for 10 s and treated under H_2 at 553, 473, and 523 K for 30 min, respectively. The horizontal axis, i_{ORR}, reflects the difference in current density between the Ar and O_2 atmospheres normalized by the molecular weight of the metal cation. The values in brackets indicate the Tafel slopes. The potential was swept cathodically at a scan rate of 5 mV s^{-1}.

The kinetics of O_2 reduction on Pt electrodes has been discussed in mainly two different potential ranges with a rotating disk electrode (RDE) system: Tafel slopes are 60 mV dec^{-1} for higher potential (>0.8 V_{RHE}) and 120 mV dec^{-1} for lower potential (<0.8 V_{RHE}).[42−44] In the case of Pt electrodes, the formation of Pt−O above 0.8 V_{RHE} reduces the Tafel slope and complicates the kinetics mechanism, resulting in a half slope.

Among the NbO_x, ZrO_x, and TaO_x nanoparticle electrodes, Tafel slopes are 133 and 102 mV dec^{-1} for ZrO_x and TaO_x, respectively. ZrO_x and TaO_x electrocatalysts are currently considered to catalyze ORR the as same as Pt catalysts without Pt−O formation.

As reported in our previous papers,[22,23] the electrodeposited TaO_x electrode shows an onset potential for the ORR close to those for commercial Pt/CB electrocatalysts. This means that

dx.doi.org/10.1021/cs400525u | ACS Catal. 2013, 3, 2181−2189

the performance of the presented electrocatalysts is comparable to that for commercial Pt/CB electrocatalysts. The presence of similar Tafel slopes for ZrO_x and TaO_x to that for bare Pt surface indicates the potential of these materials to surpass the performance of Pt electrocatalysts in the near future. On the other hand, NbO_x shows a similar Tafel slope to that for Pt catalysts, indicating that complicated reduction kinetics takes place on NbO_x catalysts, similar to the case for oxygen-contaminated Pt surfaces.

In the present method, it was difficult to prepare a RDE or rotating ring-disk electrode (RRDE) because, in the non-aqueous electrodeposition bath, a mirror-finished GC electrode cannot hold CB particles during electrodeposition. Thus, the absolute kinetic current cannot be experimentally measured without interference from mass transfer and H_2O_2 formation by 2-electron reduction. This makes it impossible to compare the performance of these electrocatalysts to those of other electrocatalysts, including commercial ones. As reported previously, the 2-electron reduction pathway is dominant especially in oxide cathode catalysts. The Tafel slopes suggest that ZrO_x and TaO_x have similar Pt catalysts without Pt−O than that of NbO_x, so that the H_2O_2 formation can be expected to be closer to Pt than NbO_x.

The loading amount in the present method is around 0.007 and 0.016 mg cm^{-2} for Zr and Ta, respectively. These amounts correspond to 1.4 and 3.2 wt % for 0.5 mg cm^{-2} of CB supported on the carbon sheet. Given that commercial Pt cathode catalysts usually have a loading amount of 20−50%, the development of highly loaded NbO_x, ZrO_x, and TaO_x electrocatalysts on CB is the next challenge.

4. CONCLUSION

In the present study, we introduced a new approach of using ultrafine (2−3 nm) oxide nanoparticles based on group IV or V metals for the ORR electrocatalysts of PEFCs. Nanoparticles of the metal oxides NbO_x, ZrO_x, and TaO_x were successfully prepared by electrodeposition in nonaqueous metal ethoxide-based solutions at room temperature. Excellent ORR activities with high onset potentials were obtained in the case of the NbO_x and ZrO_x catalysts by controlling the deposition parameters. The performance was further improved by adjusting the postelectrodeposition H_2 treatment. Physical characterization revealed that the fine oxide catalysts were deposited as a highly uniform distribution of nanoparticles, and the mixture of NbO_x and ZrO_x showed several oxidation states on the surface of the CB supports. These results were fairly consistent with those for electrodeposited TaO_x nanoparticles reported in our previous papers.[22,23] Thus, it was concluded that the high catalytic activities of the electrodeposited oxides were mainly attributable to the highly dispersed nanoparticle structure with a mixture of fully oxide and suboxide states of oxide particles on the CB. On the basis of Tafel polarization curves, the presented electrodeposited oxide nanoparticles showed similar slopes to the bare Pt catalysts and have the potential to outperform Pt group electrocatalysts.

AUTHOR INFORMATION

Corresponding Author

*E-mail: domen@chemsys.t.u-tokyo.ac.jp.

Notes

The authors declare no competing financial interest.

ACKNOWLEDGMENTS

This work was supported in part by the Funding Program for World-Leading Innovative R&D on Science and Technology (FIRST) of the Cabinet Office of Japan, the International Exchange Program of the A3 Foresight Program of the Japan Society for the Promotion of Science (JSPS), and the "Elements Strategy Initiative to Form Core Research Center" (since 2012), of the Ministry of Education, Culture, Sports, Science and Technology (MEXT), Japan. One of authors, J.S., appreciates the support of the Global Centers of Excellence (GCOE) Program of JSPS for her work at the University of Tokyo.

REFERENCES

(1) Bezerra, C. W. B.; Zhang, L.; Lee, K.; Liu, H.; Marques, A. L. B.; Marques, E. P.; Wang, H.; Zhang, J. *Electrochim. Acta* **2008**, *53*, 4937.
(2) Médard, C.; Lefèvre, M.; Dodelet, J. P.; Jaouen, F.; Lindbergh, G. *Electrochim. Acta* **2006**, *51*, 3202.
(3) Lefevre, M.; Proietti, E.; Jaouen, F.; Dodelet, J. P. *Science* **2009**, *324*, 71.
(4) Ota, K.-i.; Ohgi, Y.; Nam, K.-D.; Matsuzawa, K.; Mitsushima, S.; Ishihara, A. *J. Power Sources* **2011**, *196*, 5256.
(5) Ohnishi, R.; Takanabe, K.; Katayama, M.; Kubota, J.; Domen, K. *J. Phys. Chem. C* **2013**, *117*, 496.
(6) Kim, J. Y.; Oh, T.-K.; Shin, Y.; Bonnett, J.; Weil, K. S. *Int. J. Hydrogen Energy* **2011**, *36*, 4557.
(7) Oh, T.; Kim, J. Y.; Shin, Y.; Engelhard, M.; Weil, K. S. *J. Power Sources* **2011**, *196*, 6099.
(8) Takasu, Y.; Suzuki, M.; Yang, H.; Ohashi, T.; Sugimoto, W. *Electrochim. Acta* **2010**, *55*, 8220.
(9) Isogai, S.; Ohnishi, R.; Katayama, M.; Kubota, J.; Kim, D. Y.; Noda, S.; Cha, D.; Takanabe, K.; Domen, K. *Chem.-Asian J.* **2012**, *7*, 286.
(10) Yin, F.; Takanabe, K.; Katayama, M.; Kubota, J.; Domen, K. *Electrochem. Commun.* **2010**, *12*, 1177.
(11) Ishihara, A.; Ohgi, Y.; Matsuzawa, K.; Mitsushima, S.; Ota, K.-i. *Electrochim. Acta* **2010**, *55*, 8005.
(12) Ohgi, Y.; Ishihara, A.; Matsuzawa, K.; Mitsushima, S.; Ota, K. i.; Matsumoto, M.; Imai, H. *J. Electrochem. Soc.* **2012**, *160*, F162.
(13) Ishihara, A.; Tamura, M.; Matsuzawa, K.; Mitsushima, S.; Ota, K.-i. *J. Fuel Cell Sci. Technol.* **2011**, *8*, 031005.
(14) Rabis, A.; Rodriguez, P.; Schmidt, T. J. *ACS Catal.* **2012**, *2*, 864.
(15) Pourbaix, M. *Atlas of electrochemical equilibria in aqueous solutions*; NACE International: Houston, TX, 1974.
(16) Sasaki, K.; Takasaki, F.; Noda, Z.; Hayashi, S.; Shiratori, Y.; Ito, K. *ECS Trans.* **2012**, *33*, 473.
(17) Bezerra, C. W. B.; Zhang, L.; Liu, H.; Lee, K.; Marques, A. L. B.; Marques, E. P.; Wang, H.; Zhang, J. *J. Power Sources* **2007**, *173*, 891.
(18) Ohgi, Y.; Ishihara, A.; Matsuzawa, K.; Mitsushima, S.; Ota, K. *J. Electrochem. Soc.* **2010**, *157*, B885.
(19) Paunovic, M.; Schlesinger, M. *Fundamental of Electrochemical Deposition*; Wiley-Interscience Pub., John Wiley & Sons Inc.: New York, 1998.
(20) Simka, W.; Puszczyk, D.; Nawrat, G. *Electrochim. Acta* **2009**, *54*, 5307.
(21) Hsu, I. J.; Esposito, D. V.; Mahoney, E. G.; Black, A.; Chen, J. G. *J. Power Sources* **2011**, *196*, 8307.
(22) Seo, J.; Cha, D.; Takanabe, K.; Kubota, J.; Domen, K. *Chem. Commun.* **2012**, *48*, 9074.
(23) Seo, J.; Zhao, L.; Cha, D.; Takanabe, K.; Katayama, M.; Kubota, J.; Domen, K. *J. Phys. Chem. C* **2013**, *117*, 11635.
(24) Bard, A. J.; Parsons, R.; Jordan, J. *Standard Potentials in Aqueous Solutions, IUPAC (Marcel Dekker)*; CRC Press: New York, USA, 1985.
(25) Nam, K.-D.; Ishihara, A.; Matsuzawa, K.; Mitsushima, S.; Ota, K.-i.; Matsumoto, M.; Imai, H. *Electrochim. Acta* **2010**, *55*, 7290.
(26) Ohnishi, R.; Katayama, M.; Takanabe, K.; Kubota, J.; Domen, K. *Electrochim. Acta* **2010**, *55*, 5393.

(27) Yin, F.; Takanabe, K.; Kubota, J.; Domen, K. *J. Electrochem. Soc.* **2010**, *157*, B240.
(28) Wang, Y.; Song, S.; Maragou, V.; Shen, P. K.; Tsiakaras, P. *Appl. Catal., B* **2009**, *89*, 223.
(29) Doi, S.; Ishihara, A.; Mitsushima, S.; Kamiya, N.; Ota, K.-i. *J. Electrochem. Soc.* **2007**, *154*, B362.
(30) Hota, M. K.; Bera, M. K.; Verma, S.; Maiti, C. K. *Thin Solid Films* **2012**, *520*, 6648.
(31) Martínez-Méndez, S.; Henríquez, Y.; Domínguez, O.; D'Ornelas, L.; Krentzien, H. *J. Mol. Catal. A* **2006**, *252*, 226.
(32) Ziolek, M.; Nowak, I. *Catal. Today* **2003**, *78*, 543.
(33) Bakradze, G.; Jeurgens, L. P. H.; Mittemeijer, E. J. *J. Phys. Chem. C* **2011**, *115*, 19841.
(34) Kumari, L.; Li, W. Z.; Xu, J. M.; Leblanc, R. M.; Wang, D. Z.; Li, Y.; Guo, H.; Zhang, J. *Cryst. Growth Des.* **2009**, *9*, 3874.
(35) Liao, W.; Zheng, T.; Wang, P.; Tu, S.; Pan, W. *J. Environ. Sci.* **2010**, *22*, 1800.
(36) Miyazaki, E.; Yasumori, I. *Surf. Sci.* **1976**, *55*, 747.
(37) Nørskov, J. K.; Rossmeisl, J.; Logadottir, A.; Lindqvist, L.; Kitchin, J. R.; Bligaard, T.; Jónsson, H. *J. Phys. Chem. B* **2004**, *108*, 17886.
(38) Watanabe, E.; Ushiyama, H.; Yamashita, K. *Chem. Phys. Lett.* **2013**, *561*, 57.
(39) Day, V. W.; Klemperer, W. G.; Pafford, M. M. *Inorg. Chem.* **2001**, *40*, 5738.
(40) Bradley, D. C.; Holloway, C. E. *J. Chem. Soc. A* **1968**, 219.
(41) Wright, D. A.; Williams, D. A. *Acta Crystallogr., Sect. B* **1968**, *24*, 1107.
(42) Garsany, Y.; Epshteyn, A.; Purdy, A. P.; More, K. L.; Swider-Lyons, K. E. *J. Phys. Chem. Lett.* **2010**, *1*, 1977.
(43) Paulus, U. A.; Wokaun, A.; Scherer, G. G. *J. Phys. Chem. B* **2002**, *106*, 4181.
(44) Wakabayashi, N.; Takeichi, M.; Itagaki, M.; Uchida, H.; Watanabe, M. *J. Electroanal. Chem.* **2005**, *574*, 339.